LIMNOLOGY and OCEANOGRAPHY

ASLO

*Limnol. Oceanogr.* 9999, 2021, 1–11

doi: 10.1002/lno.11765

# Low diversity of a key phytoplankton group along the West Antarctic Peninsula

**Michael S. Brown** [1*] **Jeff S. Bowman** [2] **Yajuan Lin** [3] **Colette J. Feehan** [4] **Carly M. Moreno** [5] **Nicolas Cassar** [3] **Adrian Marchetti** [5] **Oscar M. Schofield** [1]

[1]Department of Marine and Coastal Sciences, Rutgers University, New Brunswick, New Jersey
[2]Integrative Oceanography Division, Scripps Institution of Oceanography, La Jolla, California
[3]Division of Earth and Ocean Sciences, Nicholas School of the Environment, Duke University, Durham, North Carolina
[4]Department of Biology, Montclair State University, Montclair, New Jersey
[5]Department of Marine Sciences, University of North Carolina at Chapel Hill, Chapel Hill, North Carolina

The West Antarctic Peninsula (henceforth "Peninsula") is experiencing rapid warming and melting that is impacting the regional marine food web. The primary phytoplankton groups along the Peninsula are diatoms and cryptophytes. Relative to diatoms, there has been little focus on regional cryptophytes, and thus our understanding of their diversity and ecology is limited, especially at the species level. This gap is important, as diatoms and cryptophytes play distinct roles in the regional marine food web and biogeochemistry. Here, we use a phylogenetic placement approach with 18S rRNA gene amplicon sequence variants to assess surface ocean cryptophyte diversity and its drivers at a high taxonomic resolution along the Peninsula. Data were collected over 5 years (2012–2016) during the regional research cruises of the Palmer Long-Term Ecological Research program. Our results indicate that there are two major cryptophyte taxa along the Peninsula, consisting of distinct *Geminigera* spp., which in aggregate always comprise nearly 100% of the cryptophyte community (indicating low taxa evenness). The primary taxon dominates the cryptophyte community across all samples/years, which span a broad range of oceanographic conditions. A shift in cryptophyte community composition between a lower (higher) primary (secondary) taxon percentage is associated with distinct oceanographic conditions, including lower (higher) temperature, salinity, nutrients, and cryptophyte relative abundance (phytoplankton biomass and diatom relative abundance). These results emphasize the need for a full characterization of the ecology of these two taxa, as it is predicted that cryptophytes will increase along the Peninsula given projections of continued regional environmental change.

Polar oceans play a disproportionately large role in global climate and biogeochemistry (Gruber et al. 2019). Many polar ecosystems are undergoing substantial environmental change (Meredith et al. 2019), including the West Antarctic Peninsula (henceforth "Peninsula"; Fig. 1), which is exhibiting some of the most rapid change on the planet (Schofield et al. 2010; Ducklow et al. 2013). Since the mid-20$^{th}$ century, the Peninsula has warmed considerably, including strong positive trends in oceanic temperatures (Meredith and King 2005; Martinson et al. 2008), and one of the largest increases in winter atmospheric temperatures globally (Vaughan et al. 2003). In addition, there has been widespread glacial retreat in the region (Cook et al. 2016), and the sea ice season has shortened by 3 months (Stammerjohn et al. 2012). These changes to the Peninsula are associated with changes in atmospheric circulation, in particular a deepening of the Amundsen Sea Low driven by a positive trend in the Southern Annular Mode (Fogt and Marshall 2020), which has resulted in stronger and warmer winds blowing from the north/northwest across the region (Raphael et al. 2016). Since Antarctic marine life is dependent on sea ice dynamics, these physical changes to the Peninsula have impacted the marine food web across all trophic levels (Schofield et al. 2010; Ducklow et al. 2013), including the abundance and composition of regional phytoplankton communities (Montes-Hugo et al. 2009; Sailley et al. 2013; Brown et al. 2019).

The coastal waters of the Peninsula are associated with large phytoplankton blooms during spring and summer (Smith et al. 2008). These blooms are fueled by an abundant supply of macronutrients (Kim et al. 2016). Therefore, primary

*Correspondence: mbrown@marine.rutgers.edu



Additional Supporting Information may be found in the online version of this article.

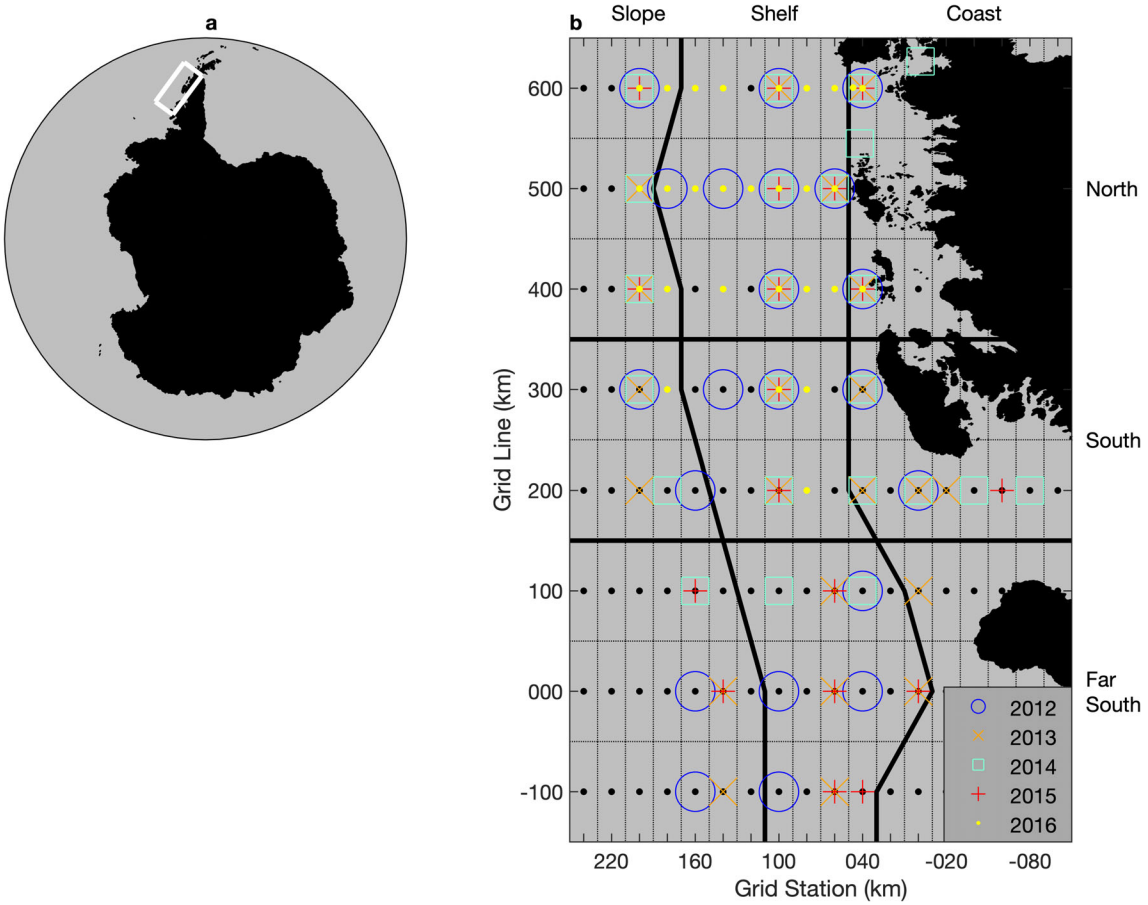


**Fig 1.** Map of the study area, including: (**a**) the Antarctic continent and (**b**) the Palmer LTER regional grid along the West Antarctic Peninsula (boxed region in **a**) with the locations of the DNA samples. The black dots and black dotted lines indicate the grid sampling stations. The black solid lines indicate along- and cross-shore subregions of the grid, which span the north, south, and far south, and coast, shelf, and slope.

production in the region is generally thought to be controlled by light availability regulated by the mixed layer depth, which in turn is driven by wind, sea ice, and meltwater dynamics (Vernet et al. 2008; Saba et al. 2014; Brown et al. 2019). Historically, the dominant phytoplankton group along the Peninsula has been considered to be diatoms, which are typically large and classified as microplankton, that is, $> 20\ \mu$m (Hart 1942). However, over the past few decades it has been recognized that smaller phytoplankton classified as nanoplankton, that is, $< 20\ \mu$m, are also important components of the regional phytoplankton community (Hewes et al. 1990; Buma et al. 1991). The dominant nanoplankton group along the Peninsula is considered to be cryptophytes (Garibotti et al. 2003; Schofield et al. 2017).

Cryptophytes are biflagellated algae, with some taxa capable of mixotrophy (Stoecker et al. 2017). Antarctic cryptophytes have been measured via microscopy to be $\sim 10\ \mu$m in size (McMinn and Hodgson 1993). It has been observed that diatoms and cryptophytes along the Peninsula do not typically co-occur and are often segregated spatially (Garibotti et al. 2003; Huang et al. 2012), and temporally, with a typical seasonal succession consisting of a diatom bloom followed by a cryptophyte bloom (Schofield et al. 2017). It has also been observed that in coastal regions of the Peninsula, the presence of cryptophytes is associated with lower salinities (Moline et al. 2004; Mendes et al. 2013; Schofield et al. 2017), and years characterized by a positive Southern Annular Mode, less sea ice, deeper mixed layer depths, and lower overall phytoplankton biomass (Saba et al. 2014). This has resulted in the prediction that the relative abundance of cryptophytes along the Peninsula will increase as the region further warms, and sea ice and glaciers continue to melt (Moline et al. 2004; Schofield et al. 2017).

Indeed, long-term analyses of phytoplankton community composition and modeled food web dynamics along the Peninsula suggest that this increase in cryptophytes is already occurring (Montes-Hugo et al. 2009; Sailley et al. 2013; Brown et al. 2019). A shift from diatoms to cryptophytes along the Peninsula could impact the regional marine food web and biogeochemistry. Specifically, due to their smaller size, cryptophytes are not as efficiently grazed by krill as diatoms (Haberman et al. 2003). Instead, salps are often associated

with smaller regional phytoplankton communities (Moline et al. 2004). Krill are an important link between phytoplankton (in particular diatoms) and higher marine trophic levels, and a decrease in regional krill populations could have negative implications for apex predators like penguins, seals, and whales (Saba et al. 2014). In addition, cryptophytes achieve lower surface ocean drawdown of atmospheric carbon dioxide relative to diatoms (Brown et al. 2019).

Although the importance of cryptophytes to phytoplankton communities along the Peninsula is recognized, they have been the focus of minimal research in the region relative to diatoms (Schofield et al. 2017). In particular, fundamental ecological questions still remain about regional cryptophytes, including the identity of their major taxa and the drivers of their diversity. Notably, although some studies have used microscopy to assess phytoplankton dynamics at the genus/species level (Mascioni et al. 2019 and references therein), most work in the region, including that of the Palmer Long-Term Ecological Research (LTER) program, has primarily focused on the use of pigment-based approaches, which only allow classification to lower taxonomic resolutions (e.g., diatoms vs. cryptophytes). However, recent studies from the Peninsula have demonstrated the importance of classifying phytoplankton at higher taxonomic resolutions when assessing their ecological and biogeochemical impacts (Luo et al. 2016; Lin et al. 2017; Rozema et al. 2017). Classifying phytoplankton at higher taxonomic resolutions also allows the determination of diversity metrics, such as richness and evenness (i.e., species number and relative abundance, respectively), that can be used to characterize spatiotemporal variability in phytoplankton community composition. As a result, the incorporation of routine molecular and quantitative imaging techniques for characterizing phytoplankton dynamics has been identified as a major priority for regional monitoring programs (Henley et al. 2019). In this study, we assess surface ocean cryptophyte diversity and its environmental drivers along the Peninsula at a high taxonomic resolution, using a phylogenetic placement approach with a 5-year data set of 18S rRNA gene sequences collected during the Palmer LTER regional research cruises.

## Methods

### Palmer LTER study area

Data for this study were collected over 5 years (2012–2016) during the Palmer LTER regional research cruises along the Peninsula, which were conducted aboard the ASRV *Laurence M. Gould* each austral summer month of January during the peak of the summer growth season. The Palmer LTER regional grid spans north to south along the Peninsula, and east to west from the coast to the continental slope (Fig. 1b). The grid consists of sampling lines 100 km apart that are oriented approximately perpendicular to the Peninsula coastline, with sampling stations located every 20 km. The grid is typically split into nine subregions, which span a broad along-shore (the north, south, and far south subregions) and cross-shore (the coast, shelf, and slope subregions) area along the Peninsula (Martinson et al. 2008).

### DNA samples

During each of the study years, DNA samples were collected over a broad along- and cross-shore area that was representative of the spatial extent of the respective Palmer LTER regional research cruise along the Peninsula (Fig. 1b). In all years, the coast, shelf, slope, north, and south subregions were sampled, and with the exception of 2016 (due to high sea ice concentrations), the far south subregion was as well. Collection and sequencing of the DNA data set has been previously described in detail (Lin et al. 2017, 2019). Briefly, seawater samples were collected from the ship's surface seawater flow-through system and were filtered onto 47-mm diameter Supor filters (0.45 $\mu$m pore size for years 2012 and 2013; 0.20 $\mu$m pore size for years 2014–2016). The filters were placed in cryovials with 1 mL of RNAlater, and then frozen and stored at −80°C. Back in the lab, each filter was removed from its cryovial and the RNAlater, and then split in half (one half for the DNA analyses discussed here; one half for unrelated RNA analyses). Next, 500 $\mu$L of RNAlater was loaded from each cryovial onto an Amicon 10k column and spun to remove the RNAlater and to concentrate any suspended cells, which were subsequently added back to the respective filter half. DNA from the filters was then extracted and purified using Qiagen DNeasy Plant Mini kits after cell lysis by bead beating with 0.1 mm Zr beads in the AP1 lysis buffer. Small subunit 18S rRNA genes were amplified by polymerase chain reaction (annealing temperature of 60°C) using the following V4 primer set: forward (5′-CCAGCASCYGCGGTAATTCC-3′) and reverse (5′-ACTTTCGTTCTTGAT-3′), which were modified from the EukF and EukR primers of Stoeck et al. (2010) for improved haptophyte coverage (Lin et al. 2017; the final three base pairs of the original reverse primer were removed).

Amplicon libraries were sequenced at the Duke University Institute for Genome Sciences and Policy using the Illumina MiSeq 300PE platform. For each amplicon library, assembly of paired-end reads was performed with *VSEARCH v2.3.4* (Rognes et al. 2016). Quality filtering and chimera checking of assembled reads was performed with *DADA2 v1.10.1* (Callahan et al. 2016). In total, 119 DNA samples were collected, but 2 were excluded due to low read counts (< 100), and 2 were excluded due to ambiguous time/location metadata, yielding 115 samples. Amplicon sequence variants (ASVs) (Callahan et al. 2017) were generated with *DADA2*, and ASVs were assigned taxonomy using the *assignTaxonomy* function (with a minimum boot strap confidence level of 50) and a *DADA2*-formatted Silva r132 reference database (Callahan 2018). Only cryptophyte ASVs, defined as those classified as *Cryptomonadales* at the phylum level in this reference database, were included in our study.

### Phylogenetic placement

The cryptophyte ASVs were further classified with a phylogenetic placement approach (Barbera et al. 2018). This method consists of placing query sequences onto a fixed reference tree using a likelihood-based algorithm (Barbera et al. 2018), which offers some advantages over other classification methods (Matsen et al. 2010). Here, we used all sequences classified as *Cryptophyceae* (the next lowest relevant taxonomic level after *Eukaryota*) in the Silva r132 reference database (Quast et al. 2013), accessed on June 12, 2019, to generate the reference tree. At the time of analysis, 2723 *Cryptophyceae* sequences were available in the Silva r132 reference database. Reference sequences were aligned with *Infernal* against the Rfam covariance model for 18S rRNA (Nawrocki and Eddy 2013) and were de-duplicated with *seqmagick* (https://fhcrc.github.io/seqmagick/), leaving 2615 unique reference sequences. These reference sequences were used to build the reference tree (Supplementary File S1) with *RAxML v8* (Stamatakis 2014) using the GTRGAMMA model. Phylogenetic placement of the cryptophyte ASVs onto the reference tree was performed with *EPA-ng* (Barbera et al. 2018). Edge distance between placement locations (EDPL) was calculated with *GUPPY* (Matsen et al. 2010). The output of the phylogenetic placement consisted of the reference tree edge to which each cryptophyte ASV was placed, and an assessment of the placement uncertainty, including EDPL and percent identity (%ID) values, where lower EDPL and higher %ID indicates lower uncertainty.

Reference tree edges (points of placement) are either terminal or internal edges. Terminal edges are defined by a unique full-length 18S rRNA gene, while internal edges represent clades. Placement to an internal edge indicates that there was insufficient phylogenetic information available for placement at a terminal edge. In that case, the taxonomy of the query sequence is considered to be the lowest consensus ranking for all reference sequences belonging to the clade. Cryptophyte taxa (e.g., TAXON1 and TAXON2 discussed below) were defined as reference tree edges to which cryptophyte ASVs were placed. For each DNA sample, (1) the read count of each cryptophyte taxon was calculated as the sum of the read counts of its corresponding cryptophyte ASVs, (2) the percentage of the cryptophyte community of each cryptophyte ASV and taxon (i.e., "cryptophyte ASV or taxon percentage") was calculated by dividing each cryptophyte ASV or taxon read count by the number of crytophyte reads, and multiplying by 100, and 3) the cryptophyte percentage of the overall eukaryotic community (i.e., "cryptophyte community percentage") was calculated by dividing the number of cryptophyte reads by the number of 18S reads, and multiplying by 100. The cryptophyte ASVs, taxa, and average ASV and taxon percentages are summarized in Supplementary Table S1

### Palmer LTER core measurements

Continuous, underway, surface ($\sim$ 5 m) temperature and salinity data collected from the ship's surface seawater flow-through system were downloaded from the Marine Geoscience Data System in files formatted according to the Joint Global Ocean Flux Study specifications. Seawater samples for macronutrients (phosphate, nitrate + nitrite, and silicate) and phytoplankton pigments, including chlorophyll *a* (Chl *a*; a primary plant pigment used as a biomass index) and accessory pigments, specifically fucoxanthin and alloxanthin (fuco and allo, respectively; the primary diatom and cryptophyte chemotaxonomic pigments), were collected from Niskin bottles deployed throughout the water column (with casts typically including 0 m, or at least one observation between 0 and 5 m), or from the ship's surface seawater flow-through system. Samples for macronutrients were filtered through combusted 47 mm diameter Whatman GF/F glass fiber filters into new plastic 15 mL centrifuge tubes, frozen and stored at −20°C, then measured by continuous flow analyzers according to Lorenzoni and Benway (2013) at the Lamont-Doherty Earth Observatory. Samples for phytoplankton pigments were filtered onto 25 mm diameter Whatman GF/F glass fiber filters and wrapped in foil. Filters for Chl *a* via fluorescence were frozen and stored at −80°C, then measured according to Parsons et al. (1984) at either Palmer Station (2012–2015) or Rutgers University (2016). Filters for Chl *a* and accessory pigments via high performance liquid chromatography (HPLC) were flash frozen in liquid nitrogen, stored at −80°C, then measured according to Kozlowski et al. (2011) at Rutgers University. Due to a freezer failure, HPLC data are not available for 2012.

Data were quality-controlled by excluding observations with values outside of realistic environmental ranges according to Brown et al. (2019), including temperature: −2°C to 4°C; salinity: 30–42; phosphate: 0–5 $\mu$mol $L^{-1}$; nitrate + nitrite: 0–50 $\mu$mol $L^{-1}$; silicate: 0–175 $\mu$mol $L^{-1}$; Chl *a*: 0–60 mg $m^{-3}$. For each sampling event, replicate macronutrients and phytoplankton pigments observations per depth were depth-averaged, and surface averages were calculated by averaging any observations between 0 and 5 m. For each DNA sample, corresponding surface values of temperature, salinity, macronutrients, and phytoplankton pigments were constructed by (1) averaging any surface temperature and salinity observations within 1 h and (2) averaging any surface averages of macronutrients and phytoplankton pigments within 1 d and 10 km, or if no observations met these criteria, 20 km (the half and full distance between sampling stations, respectively; Fig. 1b).

### Seascape units

The corresponding physicochemical and biological oceanographic conditions of the DNA samples were contextualized using the eight recurrent seascape units (SUs) along the Peninsula defined by Bowman et al. (2018). Briefly, Bowman et al. (2018) trained a self-organizing map on a data set of regional temperature, salinity, macronutrients, and Chl *a* collected by the Palmer LTER program. The self-organizing map units were further segmented using k-means clustering to

**Table 1.** Summary of the relevant physicochemical and biological attributes (temperature: T, salinity: S, phosphate: P, nitrate + nitrite: N, and chlorophyll *a*: Chl *a*), and typical locations within the Palmer LTER regional grid, of the primary seascape units (SUs) associated with the DNA sample data set (SU1, SU6, and SU8). Refer to Table 1 of Bowman et al. (2018) for further information on these and the other five SUs that appear along the West Antarctic Peninsula. The DNA samples were classified into two groups (GROUP1 and GROUP2), which were defined based on the TAXON1 percentage of the cryptophyte community: GROUP1 (TAXON1 > 95%); GROUP2 (TAXON1 < 95%). While GROUP1 was primarily associated with SU1 and SU8, GROUP2 was primarily associated with SU6.

| | T (°C) | S | P ($\mu$mol $L^{-1}$) | N ($\mu$mol $L^{-1}$) | Chl *a* (mg $m^{-3}$) | Location |
|---|---|---|---|---|---|---|
| SU1 | 1.02 | 33.80 | 1.38 | 19.99 | 0.55 | Mainly the upper surface ocean west of the 100 line. |
| SU6 | 0.21 | 33.14 | 0.96 | 14.23 | 8.51 | Mainly the upper surface ocean east of the 100 line. |
| SU8 | 0.52 | 33.62 | 1.54 | 22.60 | 1.13 | Mainly the northern and eastern surface ocean, but widespread. |

generate eight clusters, that is, SUs, each defining a distinct parameter space (Table 1). The output of the segmentation is a classification model that can be used to assign one the eight SUs to new observations. Bowman et al. (2018) used the classification model to assign SUs to a long-term data set of observations along the Peninsula to examine the spatiotemporal variability of the SUs. Here, we used the classification model to determine the SU of each DNA sample with the corresponding surface values of temperature, salinity, macronutrients, and Chl *a* via fluorescence, using the *map* function in the R package *kohonen* (Wehrens and Kruisselbrink 2018). While additional oceanographic variables may also be relevant, the SUs represent an efficient and comprehensive means to simultaneously characterize both physical and ecological oceanographic conditions.

## Results

### Cryptophyte ASVs and taxa

In total, 94 cryptophyte ASVs were identified in the 18S rRNA gene amplicon libraries (Supplementary Table S1). However, only two ASVs (henceforth ASV1 and ASV2) contributed substantially to the cryptophyte community, in aggregate always comprising > 90% of the cryptophyte reads (except for one sample). Specifically, ASV1 was the primary ASV (ASV percentage always > 70%; average ASV percentage of 91%), followed by ASV2 (average ASV percentage of 4%). All the other ASVs did not reach an average ASV percentage of 1%. Phylogenetic placement of the cryptophyte ASVs onto the reference tree yielded 25 distinct points of placement, that is, cryptophyte taxa (Fig. 2; Supplementary File S1 and Table S1). However, only two taxa (henceforth TAXON1 and TAXON2) contributed substantially to the cryptophyte community, in aggregate always comprising > 98% of the cryptophyte reads. Specifically, TAXON1 was the primary taxon (taxon percentage always > 70%; average taxon percentage of 96%), followed by TAXON2 (average taxon percentage of 4%). All the other taxa did not reach an average taxon percentage of 1%. TAXON1 consisted of 58 ASVs, including ASV1. This taxon corresponded to an internal node of the reference tree (Edge #5196), which was comprised of both an uncultured *Geminigera* species from the South Atlantic (FJ032651) and a *Geminigera cryophila* strain from Ace Lake, Antarctica (HQ111513). TAXON2 consisted of just ASV2. This taxon corresponded to a terminal node of the reference tree (Edge #5226), which was a *G. cryophila* strain from an unspecified location (AB058366). Notably, strain AB058366 was identical after alignment to a NCMA *G. cryophila* strain from McMurdo Sound, Antarctica (CCMP2564), which was not included in the Silva r132 reference database (Quast et al. 2013). Placements to both Edge #5196 and #5226 were of high confidence, as indicated by both low EDPLs and high % IDs (Edge #5196: EDPL = $3 \times 10^{-3}$, %ID = 93–98%; Edge #5226: EDPL = $2 \times 10^{-4}$, %ID = 100%).

### Drivers of cryptophyte diversity

There was a clear inverse relationship between the percentage of the cryptophyte community of TAXON1 and TAXON2,

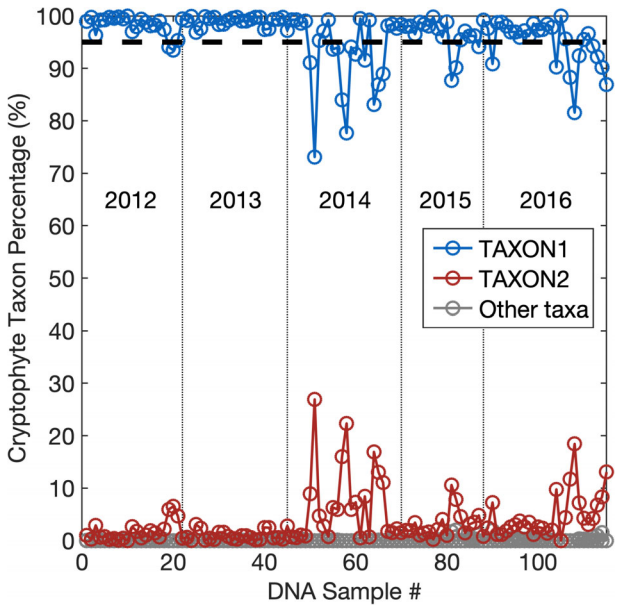


**Fig 2.** Percentage of the cryptophyte community of the two primary cryptophyte taxa (TAXON1 and TAXON2), and all other taxa, for each of the DNA samples. The black horizontal dashed line indicates a cryptophyte taxon percentage of 95%.

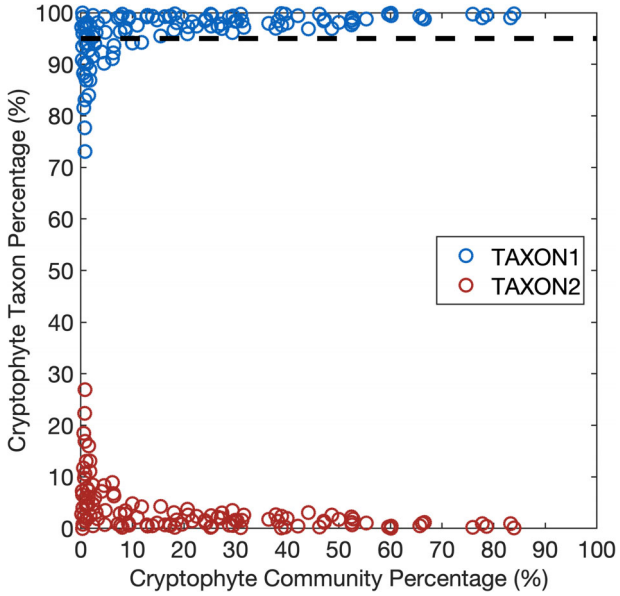


**Fig 3.** Percentage of the cryptophyte community of the two primary cryptophyte taxa (TAXON1 and TAXON2) plotted vs. the cryptophyte percentage of the overall eukaryotic community. The black horizontal dashed line indicates a cryptophyte taxon percentage of 95%.

the two major cryptophyte taxa (Fig. 2). Specifically, while TAXON1 was consistently dominant (taxon percentage always > 70%), a decrease in the TAXON1 taxon percentage coincided with an increase in the TAXON2 taxon percentage. This shift in cryptophyte community composition was most substantial when cryptophytes were a small percentage (< 10%) of the overall eukaryotic community (Fig. 3). To identify additional physicochemical and biological oceanographic conditions associated with the shift between TAXON1 and TAXON2 (with the SUs and phytoplankton accessory pigment data), the DNA samples were separated into two groups (henceforth GROUP1 and GROUP2), based on the TAXON1 percentage of the cryptophyte community. Specifically, GROUP1 was defined as where TAXON1 > 95%, and GROUP2 was defined as where TAXON1 < 95% (see the black horizontal dashed line in Figs. 2 and 3).

In total, six of the eight recurrent SUs along the Peninsula identified by Bowman et al. (2018) were associated with the DNA samples, including SU1, SU2, SU3, SU5, SU6, and SU8 (Fig. 4). The primary SUs represented were SU1, SU6, and SU8, which accounted for 29%, 35%, and 29% of the samples, respectively. Notably, unlike the SUs not represented at all

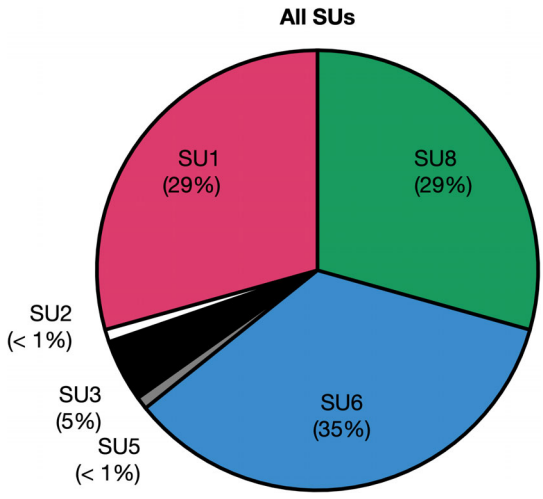


**Fig 4.** Seascape units (SUs) represented by the full DNA sample data set; *n* = 109.

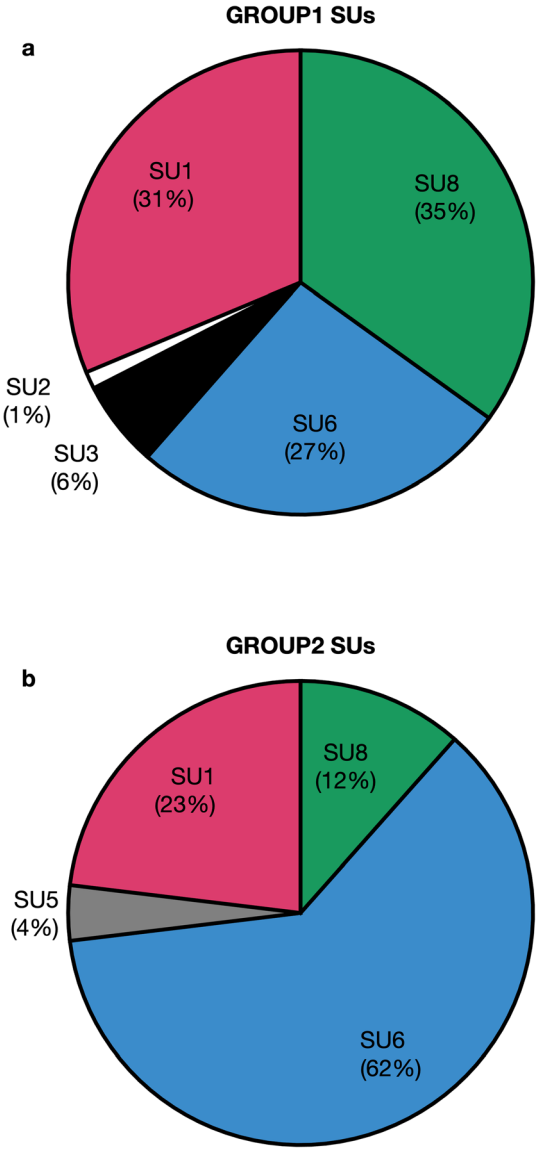


**Fig 5.** Seascape units (SUs) represented by DNA samples classified as either of the two groups (GROUP1 and GROUP2), which were defined based on the TAXON1 percentage of the cryptophyte community: (**a**) GROUP1 (TAXON1 > 95%), *n* = 83; (**b**) GROUP2 (TAXON1 < 95%), *n* = 26.

(SU4 and SU7), the primary SUs represented (SU1, SU6, and SU8) are frequently observed in the surface ocean along the Peninsula (Table 1; Bowman et al. 2018). To assess differences in the SU composition associated with GROUP1 and GROUP2, a chi-square test was performed. A single bin was used for the SUs that were less represented (SU2, SU3, and SU5), or not represented at all (SU4 and SU7). There was a significant difference in the SU relative frequencies of GROUP1 and GROUP2 ($\chi^2$ = 11.5, $p$ = 0.009, df = 3; Fig. 5). Specifically, while both GROUP1 and GROUP2 primarily occurred in conditions characterized as SU1, SU6, and SU8 (93% and 97% of samples, respectively), GROUP1 was mainly associated with SU1 and SU8 (together 66% of samples) and GROUP2 was mainly associated with SU6 (62% of samples). Notably, relative to both SU1 and SU8, SU6 is characterized by distinct physicochemical and biological oceanographic conditions, including lower temperature, salinity, phosphate, and nitrate + nitrite, and higher Chl *a* (Table 1).

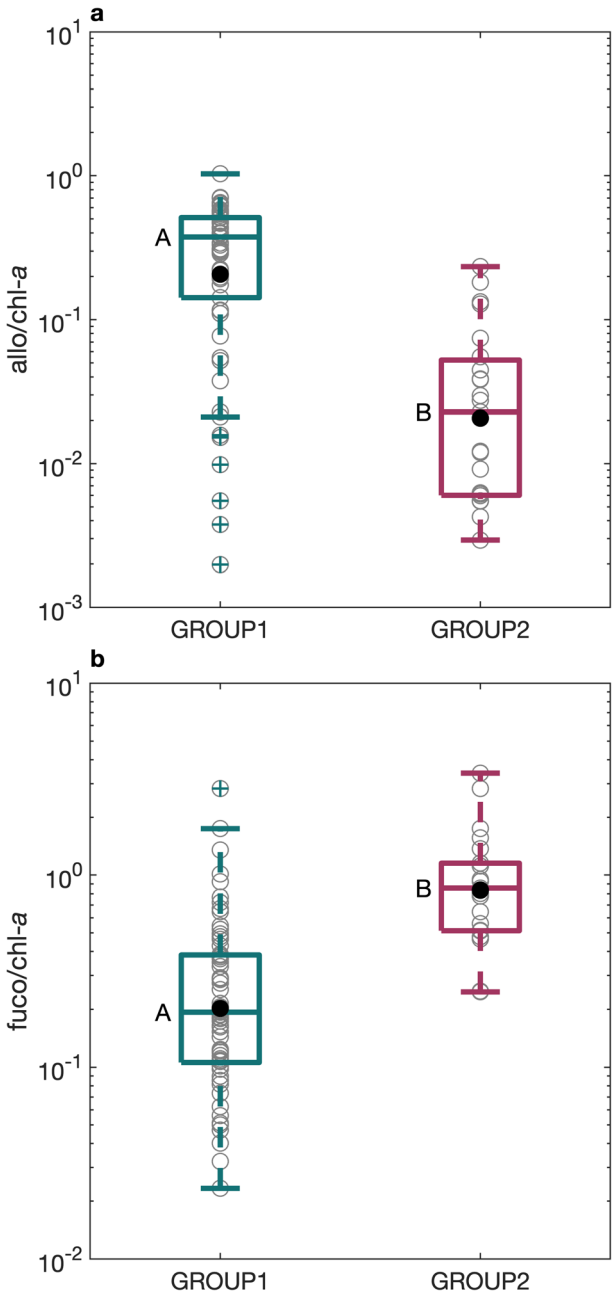


**Fig 6.** The ratio to chlorophyll *a* (Chl *a*) via HPLC of (**a**) alloxanthin (allo) and (**b**) fucoxanthin (fuco) for DNA samples classified as either of the two groups (GROUP1 and GROUP2), which were defined based on the TAXON1 percentage of the cryptophyte community: GROUP1 (TAXON1 > 95%), $n$ = 66 and 65 in (**a**) and (**b**); GROUP2 (TAXON1 < 95%), $n$ = 23 and 23 in (**a**) and (**b**). The horizontal lines indicate the median and 25$^{th}$ and 75$^{th}$ percentiles, and the black circles indicate the mean. The gray circles indicate individual values. The whiskers extend to values not considered as outliers, with outliers indicated by colored pluses. The presence of a difference among groups was determined with Welch's *t*-tests, and the capital letters indicate statistical groupings at $\alpha$ = 0.05.

To assess differences in phytoplankton accessory pigments associated with GROUP1 and GROUP2, two-tailed Welch's *t*-tests were performed on their respective allo/Chl *a* and fuco/Chl *a* via HPLC ratios. The phytoplankton pigment ratios were $\log_{10}$-transformed prior to analysis to ensure normality. A single fuco/Chl *a* ratio was excluded due to a fuco value of 0 mg m$^{-3}$. Relative to GROUP1, GROUP2 was associated with a significantly lower allo/Chl *a* ratio and a significantly higher fuco/Chl *a* ratio ($t$ = 7.0, $p$ < 0.001, df = 40.2 and $t$ = −7.6, $p$ < 0.001, df = 60.7, respectively; Fig. 6). Finally, examination of the spatiotemporal distribution of GROUP1 and GROUP2 indicated that while GROUP1 occurred throughout the Palmer LTER regional grid, GROUP2 occurred further onshore in the north and south subregions, and further offshore in the far south subregion (Supplementary Fig. S1), and primarily later in the time series, especially in 2014 and 2016 (Fig. 2).

## Discussion

This study indicates that there is a low diversity of cryptophytes in the surface ocean along the Peninsula. As with diatoms, cryptophytes are a key phytoplankton group in the region (Garibotti et al. 2003; Schofield et al. 2017). Here, we define diversity primarily in terms of evenness, given the clearly unequal distribution of the cryptophyte community members. Specifically, of the 94 cryptophyte ASVs identified in the DNA samples, just 2 (ASV1 and ASV2) contribute substantially to the cryptophyte community, in aggregate essentially always comprising > 90% of cryptophyte reads (Supplementary Table S1). Furthermore, of the 25 cryptophyte taxa identified by phylogenetic placement of the cryptophyte ASVs, just two (TAXON1 and TAXON2) contribute substantially to the cryptophyte community, in aggregate always comprising > 98% of the cryptophyte reads (Fig. 2; Supplementary Table S1). Therefore, while regional cryptophytes have nonnegligible richness, it does not appear to be substantially functional. For comparison, regional diatoms have a higher diversity in terms of both richness (~ 600

ASVs) and evenness (~ 20 ASVs that contribute substantially to the diatom community) than cryptophytes (Yajuan Lin unpubl. data).

The primary cryptophyte taxon along the Peninsula is TAXON1, which always comprises > 70% of the cryptophyte reads (average taxon percentage of 96%; Fig. 2, Supplementary Table S1). This taxon closely matches a *G. cryophila* strain from Ace Lake, Antarctica (HQ111513). The DNA samples used for this study were collected over a broad spatiotemporal extent (Fig. 1b) that sufficiently covered the surface ocean along the Peninsula. Specifically, six of the eight regionally recurrent SUs identified by Bowman et al. (2018) were represented by the DNA samples (Fig. 4), and the remaining two SUs do not typically occur in the surface ocean. This indicates that TAXON1 is capable of dominating the regional cryptophyte community over a wide range of oceanographic conditions. The secondary cryptophyte taxon along the Peninsula is TAXON2 (average taxon percentage of 4%; Fig. 2, Supplementary Table S1), which closely matches a *G. cryophila* strain from McMurdo Sound, Antarctica (CCMP2564).

While certainly intriguing, it is not unexpected that the primary cryptophyte taxon along the Peninsula closely matches a cryptophyte strain from Ace Lake. Located in the Vestfold Hills of East Antarctica < 200 m from the nearest marine inlet, Ace Lake is a meromictic (permanently stratified) saline (mixolimnion salinity ranges ~ 11 to 30) lake that only recently (~ 5000 years ago) became fully separated from the ocean (Laybourn-Parry and Bell 2014). The fact that TAXON1 closely matches the Ace Lake *G. cryophila* strain is consistent with observations from around Antarctica (including the Peninsula) that coastal marine cryptophytes display a tolerance for lower salinities (Moline et al. 2004; Mendes et al. 2013; Schofield et al. 2017). In addition, the Ace Lake *G. cryophila* strain has been observed to contribute substantially to the coastal phytoplankton communities of King George Island in the Northern Peninsula (Luo et al. 2016). Interestingly, while both TAXON1 and TAXON2 belong to the cryptophyte genus *Geminigera*, the few previous cryptophyte blooms along the Peninsula observed via microscopy were identified as belonging either to the cryptophyte genera *Cryptomonas* or *Teleaulax* (Mascioni et al. 2019 and references therein). It should be noted that both the *Cryptomonas* and *Teleaulax* genera were represented in the DADA2-formatted Silva r132 reference database used to assign taxonomy to ASVs (Callahan 2018), and the Silva r132 *Cryptophyceae* reference database used for the phylogenetic placement of cryptophyte ASVs (Quast et al. 2013). This emphasizes the need for future studies pairing molecular and microscopy techniques to identify regional cryptophytes, and a focus on adding regional sequences to reference databases.

Variability in cryptophyte community composition along the Peninsula is primarily associated with changes in the percentage of the cryptophyte community of the two major cryptophyte taxa. Specifically, a decrease in the TAXON1 taxon percentage coincides with an increase in the TAXON2 taxon percentage (Fig. 2). Separating the DNA samples into two groups (GROUP1 and GROUP2) based on the TAXON1 percentage of the cryptophyte community (GROUP1: TAXON1 > 95%; GROUP2: TAXON1 < 95%) indicates that this shift in cryptophyte community composition is related to changes in oceanographic physicochemical and biological conditions. In particular, relative to GROUP1, GROUP2 is primarily associated with SU6 rather than SU1 and SU8 (Fig. 5). Therefore, the shift to a lower (higher) TAXON1 (TAXON2) taxon percentage coincides with lower temperature, salinity, and macronutrients, and higher phytoplankton biomass. Notably, the spatial distribution of GROUP1 and GROUP2 (Supplementary Fig. S1) is consistent with the long-term spatial distribution of the SUs, where in the north and south subregions (Fig. 1b), SU1 typically occurs further offshore, SU6 further onshore, and SU8 is widespread (Bowman et al. 2018; their analysis did not include the far south subregion). There is temporal variability in the occurrence of GROUP1 and GROUP2 (Fig. 2), although the relatively short length of the DNA data set prevents meaningful trends to be determined.

In addition, relative to GROUP1, GROUP2 is associated with a lower relative abundance of cryptophytes (Figs. 3, 6a) and a higher relative abundance of diatoms (Fig. 6b). This observation is also supported by the fact that, based on the DNA sequences, there is a significant negative correlation ($r = -0.64$, $p < 0.001$) between the diatom and cryptophyte community percentages (Yajuan Lin unpubl. data). Therefore, the shift to a lower (higher) TAXON1 (TAXON2) percentage also coincides with a shift from cryptophytes to diatoms. These results are consistent with previous observations that relative to cryptophyte assemblages, diatom assemblages along the Peninsula are associated with lower macronutrients and higher phytoplankton biomass (Brown et al. 2019), and that these two phytoplankton groups do not typically co-occur (Garibotti et al. 2003; Huang et al. 2012; Schofield et al. 2017). Ultimately, this study indicates that the primary cryptophyte taxon along the Peninsula contributes most substantially to the cryptophyte community during less productive conditions when cryptophytes have a higher relative abundance. The primary taxon contributes less to the cryptophyte community (and is replaced by the secondary taxon) during more productive conditions when cryptophytes have a lower relative abundance (and have been replaced by diatoms).

The Peninsula marine ecosystem is structured by complex atmosphere-ice-ocean dynamics (Ducklow et al. 2013), and there is uncertainty in how the region will respond to continued global change (Henley et al. 2019). For example, although the Southern Annular Mode has recently trended positive, it is unclear how opposing effects of the ozone hole recovery and increased greenhouse gas concentrations will ultimately impact its phase and seasonality (Fogt and Marshall 2020). In addition, it has been observed that long-term trends in atmospheric warming and sea ice decline have slowed (Turner

et al. 2016; Schofield et al. 2018), although they remain significant since the second half of the 20th century (Henley et al. 2019), and the trends in oceanic warming and glacial retreat show no evidence of slowing (Cook et al. 2016). Therefore, it is generally predicted that the Peninsula will continue to warm and melt.

The Peninsula is currently characterized by a meridional climate gradient. Specifically, while the mid/southern Peninsula remains a dry polar system, the northern Peninsula has been altered such that it now represents a more maritime subpolar system (Ducklow et al. 2013). In the north, warming, glacial retreat, and sea ice decline have driven bottom-up effects on the Peninsula marine ecosystem, resulting in declines in phytoplankton biomass and cell size, a community shift from diatoms to cryptophytes, and an increasingly microbially-dominated food web (Montes-Hugo et al. 2009; Sailley et al. 2013; Brown et al. 2019). It is predicted that these northern conditions will expand as the effects of climate change progress southward along the Peninsula (Henley et al. 2019). These changes to the Peninsula marine ecosystem could reinforce the substantial contribution of the primary cryptophyte taxon to the regional cryptophyte community, resulting in continued low regional cryptophyte diversity, given the association of this taxon with less productive conditions and the occurrence of cryptophytes. Future studies should focus on assessing phytoplankton diversity along the Peninsula at a high taxonomic resolution, with a particular emphasis on characterizing the ecology of these two major cryptophyte taxa in the context of regional environmental change.

### Data Availability Statement

The surface flow-through temperature and salinity data set is available from the Marine Geoscience Data System, http://www.marine-geo.org/index.php. The Palmer LTER data set is available from the Palmer LTER Data System, https://pal.lternet.edu/data. The DNA data set has been deposited in the National Center for Biotechnology Information (NCBI) Sequence Read Archive database under accession number PRJNA508517.

## References


Barbera, P., A. M. Kozlov, L. Czech, B. Morel, D. Darriba, T. Flouri, and A. Stamatakis. 2018. EPA-ng: Massively parallel evolutionary placement of genetic sequences. Syst. Biol. **68**: 365–369. doi:10.1093/sysbio/syy054

Bowman, J. S., M. T. Kavanaugh, S. C. Doney, and H. W. Ducklow. 2018. Recurrent seascape units identify key ecological processes along the western Antarctic Peninsula. Glob. Change Biol. **24**: 3065–3078. doi:10.1111/gcb.14161

Brown, M. S., D. R. Munro, C. J. Feehan, C. Sweeney, H. W. Ducklow, and O. M. Schofield. 2019. Enhanced oceanic $CO_2$ uptake along the rapidly changing West Antarctic Peninsula. Nat. Clim. Change. **9**: 678–683. doi:10.1038/s41558-019-0552-3

Buma, A. G. J., H. J. W. de Baar, R. F. Nolting, and A. J. van Bennekom. 1991. Metal enrichment experiments in the Weddell-Scotia Seas: Effects of iron and manganese on various plankton communities. Limnol. Oceanogr. **36**: 1865–1878.

Callahan, B. J., P. J. McMurdie, M. J. Rosen, A. W. Han, A. J. Johnson, and S. P. Holmes. 2016. DADA2: High-resolution sample inference from Illumina amplicon data. Nat. Methods **13**: 581–583. doi:10.1038/nmeth.3869

Callahan, B. J., P. J. McMurdie, and S. P. Holmes. 2017. Exact sequence variants should replace operational taxonomic units in marker-gene data analysis. ISME J. **11**: 2639–2643. doi:10.1038/ismej.2017.119

Callahan, B. J. 2018. Silva taxonomic training data formatted for DADA2 (Silva version 132). Zenodo. doi:10.5281/zenodo.1172783

Cook, A. J., P. R. Holland, M. P. Meredith, T. Murray, A. Luckman, and D. G. Vaughan. 2016. Ocean forcing of glacier retreat in the western Antarctic Peninsula. Science **353**: 283–286. doi:10.1126/science.aae0017

Ducklow, H. W., and others. 2013. West Antarctic Peninsula: An ice-dependent coastal marine ecosystem in transition. Oceanography **26**: 190–203. doi:10.5670/oceanog.2013.62

Fogt, R. L., and G. J. Marshall. 2020. The southern annular mode: Variability, trends, and climate impacts across the southern hemisphere. WIREs Clim. Change. **11**: e652. doi:10.1002/wcc.652

Garibotti, I. A., M. Vernet, M. E. Ferrario, R. C. Smith, R. M. Ross, and L. B. Quetin. 2003. Phytoplankton spatial distribution patterns along the western Antarctic Peninsula (Southern Ocean). Mar. Ecol. Prog. Ser. **261**: 21–39. doi:10.3354/meps261021

Gruber, N., P. Landschützer, and N. S. Lovenduski. 2019. The variable Southern Ocean carbon sink. Ann. Rev. Mar. Sci. **11**: 159–186. doi:10.1146/annurev-marine-121916-063407

Haberman, K. L., R. M. Ross, and L. B. Quetin. 2003. Diet of the Antarctic krill (*Euphausia superba* Dana): II. Selective grazing in mixed phytoplankton assemblages. J. Exp. Mar. Biol. Ecol **283**: 97–113. doi:10.1016/S0022-0981(02)00467-7

Hart, T. J. 1942. Phytoplankton periodicity in the Antarctic surface waters. Discovery Rep. **21**: 261–356.

Henley, S. F., and others. 2019. Variability and change in the West Antarctic Peninsula marine system: Research priorities and opportunities. Prog. Oceanogr. **173**: 208–237. doi:10.1016/j.pocean.2019.03.003

Hewes, C. D., E. Sakshaug, F. M. H. Reid, and O. Holm-Hansen. 1990. Microbial autotrophic and heterotrophic eucaryotes in Antarctic waters: Relationships between biomass and chlorophyll, adenosine triphosphate and particulate organic carbon. Mar. Ecol. Prog. Ser. **63**: 27–35.

Huang, K., H. Ducklow, M. Vernet, N. Cassar, and M. L. Bender. 2012. Export production and its regulating factors

in the West Antarctica Peninsula region of the Southern Ocean. Global Biogeochem. Cycles **26**: GB2005. doi:10.1029/2010GB004028

Kim, H., S. C. Doney, R. A. Iannuzzi, M. P. Meredith, D. G. Martinson, and H. W. Ducklow. 2016. Climate forcing for dynamics of dissolved inorganic nutrients at Palmer Station, Antarctica: An interdecadal (1993–2013) analysis. Eur. J. Vasc. Endovasc. Surg. **121**: 2369–2389. doi:10.1002/2015JG003311

Kozlowski, W. A., D. Deutschman, I. Garibotti, C. Trees, and M. Vernet. 2011. An evaluation of the application of CHEMTAX to Antarctic coastal pigment data. Deep-Sea Res. Part I Oceanogr. Res. Pap. **58**: 350–364. doi:10.1016/j.dsr.2011.01.008

Laybourn-Parry, J., and E. M. Bell. 2014. Ace Lake: Three decades of research on a meromictic, Antarctic lake. Polar Biol. **37**: 1685–1699. doi:10.1007/s00300-014-1553-3

Lin, Y., N. Cassar, A. Marchetti, C. Moreno, H. Ducklow, and Z. Li. 2017. Specific eukaryotic plankton are good predictors of net community production in the Western Antarctic Peninsula. Sci. Rep. **7**: 14845. doi:10.1038/s41598-017-14109-1

Lin, Y., S. Gifford, H. Ducklow, O. Schofield, and N. Cassar. 2019. Towards quantitative microbiome community profiling using internal standards. Appl. Environ. Microbiol. **85**: e02634–e02618. doi:10.1128/AEM.02634-18

Lorenzoni, L., and H. M. Benway [eds.]. 2013. Global intercomparability in a changing ocean: An international time-series methods workshop, November 28–30, 2012; Bermuda Institute of Ocean Sciences, St. Georges, Bermuda; Ocean Carbon and Biogeochemistry (OCB) Program and International Ocean Carbon Coordination Project (IOCCP). doi:10.25607/OBP-12

Luo, W., H. Li, S. Gao, Y. Yu, L. Lin, and Y. Zeng. 2016. Molecular diversity of microbial eukaryotes in sea water from Fildes Peninsula, King George Island. Antarctica. Polar Biol. **39**: 605–616. doi:10.1007/s00300-015-1815-8

Martinson, D. G., S. E. Stammerjohn, R. A. Iannuzzi, R. Smith, and M. Vernet. 2008. Western Antarctic Peninsula physical oceanography and spatio-temporal variability. Deep-Sea Res. Part II Top. Stud. Oceanogr. **55**: 1964–1987. doi:10.1016/j.dsr2.2008.04.038

Mascioni, M., G. O. Almandoz, A. O. Cefarelli, A. Cusick, M. E. Ferrario, and M. Vernet. 2019. Phytoplankton composition and bloom formation in unexplored nearshore waters of the western Antarctic Peninsula. Polar Biol. **42**: 1859–1872. doi:10.1007/s00300-019-02564-7

Matsen, F. A., R. B. Kodner, and E. V. Armbrust. 2010. Pplacer: Linear time maximum-likelihood and Bayesian phylogenetic placement of sequences onto a fixed reference tree. BMC Bioinf. **11**: 538. doi:10.1186/1471-2105-11-538

McMinn, A., and D. Hodgson. 1993. Summer phytoplankton succession in Ellis Fjord, eastern Antarctica. J. Plankton Res. **15**: 925–938. doi:10.1093/plankt/15.8.925

Mendes, C. R. B., V. M. Tavano, M. C. Leal, M. S. de Souza, V. Brotas, and C. A. E. Garcia. 2013. Shifts in the dominance between diatoms and cryptophytes during three late summers in the Bransfield Strait (Antarctic Peninsula). Polar Biol. **36**: 537–547. doi:10.1007/s00300-012-1282-4

Meredith, M., and others. 2019. Polar regions, p. 231–320. *In* H.-O. Pörtner and others [eds.], IPCC special report on the ocean and cryosphere in a changing climate.

Meredith, M. P., and J. C. King. 2005. Rapid climate change in the ocean west of the Antarctic Peninsula during the second half of the 20th century. Geophys. Res. Lett. **32**: L19604. doi:10.1029/2005GL024042

Moline, M., H. Claustre, T. K. Frazer, O. Schofield, and M. Vernet. 2004. Alteration of the food web along the Antarctic Peninsula in response to a regional warming trend. Glob. Chang. Biol. **10**: 1973–1980. doi:10.1111/j.1365-2486.2004.00825.x

Montes-Hugo, M. A., and others. 2009. Recent changes in phytoplankton communities associated with rapid regional climate change along the Western Antarctic Peninsula. Science **323**: 1470–1473. doi:10.1126/science.1164533

Nawrocki, E. P., and S. R. Eddy. 2013. Infernal 1.1: 100-fold faster RNA homology searches. Bioinformatics **29**: 2933–2935. doi:10.1093/bioinformatics/btt509

Parsons, R. T., Y. Maita, and C. M. Lalli. 1984. A manual of chemical and biological methods for seawater analysis. Pergammon Press.

Quast, C., E. Pruesse, P. Yilmaz, J. Gerken, T. Schweer, P. Yarza, J. Peplies, and F. O. Glöckner. 2013. The SILVA ribosomal RNA gene database project: Improved data processing and web-based tools. Nucl. Acids Res. **41**: D590–D596. doi:10.1093/nar/gks1219

Raphael, M. N., and others. 2016. The Amundsen Sea low: Variability, change, and impact on Antarctic climate. Bull. Am. Meteorol. Soc. **97**: 111–121. doi:10.1175/BAMS-D-14-00018.1

Rognes, T., T. Flouri, B. Nichols, C. Quince, and F. Mahé. 2016. VSEARCH: A versatile open source tool for metagenomics. PeerJ. **4**: e2584. doi:10.7717/peerj.2584

Rozema, P. D., T. Biggs, P. A. A. Sprong, A. G. J. Buma, H. J. Venables, C. Evans, M. P. Meredith, and H. Bolhuis. 2017. Summer microbial community composition governed by upper-ocean stratification and nutrient availability in northern Marguerite Bay. Antarct. Deep Sea Res. Pt. II Top. Stud. Oceanogr. **139**: 151–166. doi:10.1016/j.dsr2.2016.11.016

Saba, G. K., and others. 2014. Winter and spring controls on the summer food web of the coastal West Antarctic Peninsula. Nat. Commun. **5**: 4318. doi:10.1038/ncomms5318

Sailley, S. F., H. W. Ducklow, H. V. Moeller, W. R. Fraser, O. M. Schofield, D. K. Steinberg, L. M. Garzio, and S. C. Doney. 2013. Carbon fluxes and pelagic ecosystem dynamics near two western Antarctic Peninsula Adélie penguin

colonies: An inverse model approach. Mar. Ecol. Prog. Ser. **492**: 253–272. doi:10.3354/meps10534

Schofield, O., H. W. Ducklow, D. G. Martinson, M. P. Meredith, M. A. Moline, and W. R. Fraser. 2010. How do polar marine ecosystems respond to rapid climate change? Science **328**: 1520–1523. doi:10.1126/science.1185779

Schofield, O., and others. 2017. Decadal variability in coastal phytoplankton community composition in a changing West Antarctic Peninsula. Deep-Sea Res. Part I Oceanogr. Res. Pap **124**: 42–54. doi:10.1016/j.dsr.2017.04.014

Schofield, O., and others. 2018. Changes in the upper ocean mixed layer and phytoplankton productivity along the West Antarctic Peninsula. Philos. Trans. R. Soc. A Math. Phys. Eng. Sci. **376**: 20170173. doi:10.1098/rsta.2017.0173

Smith, R., D. G. Martinson, S. E. Stammerjohn, R. A. Iannuzzi, and K. Ireson. 2008. Bellingshausen and western Antarctic Peninsula region: Pigment biomass and sea-ice spatial/temporal distributions and interannual variabilty. Deep-Sea Res. Part II Top. Stud. Oceanogr. **55**: 1949–1963. doi:10.1016/j.dsr2.2008.04.027

Stamatakis, A. 2014. RAxML version 8: A tool for phylogenetic analysis and post-analysis of large phylogenies. Bioinformatics **30**: 1312–1313. doi:10.1093/bioinformatics/btu033

Stammerjohn, S., R. Massom, D. Rind, and D. Martinson. 2012. Regions of rapid sea ice change: An inter-hemispheric seasonal comparison. Geophys. Res. Lett. **39**: L06501. doi:10.1029/2012GL050874

Stoeck, T., D. Bass, M. Nebel, R. Christen, M. D. M. Jones, H. W. Breiner, and T. A. Richards. 2010. Multiple marker parallel tag environmental DNA sequencing reveals a highly complex eukaryotic community in marine anoxic water. Mol. Ecol. **19**: 21–31. doi:10.1111/j.1365-294X.2009.04480.x

Stoecker, D. K., P. J. Hansen, D. A. Caron, and A. Mitra. 2017. Mixotrophy in the marine plankton. Ann. Rev. Mar. Sci. **9**: 311–335. doi:10.1146/annurev-marine-010816-060617

Turner, J., and others. 2016. Absence of 21st century warming on Antarctic Peninsula consistent with natural variability. **535**: 411–415. doi:10.1038/nature18645

Vaughan, D. G., and others. 2003. Recent rapid regional climate warming on the Antarctic Peninsula. Clim. Change **60**: 243–274. doi:10.1023/A:1026021217991

Vernet, M., D. Martinson, R. Iannuzzi, S. Stammerjohn, W. Kozlowski, K. Sines, R. Smith, and I. Garibotti. 2008. Primary production within the sea-ice zone west of the Antarctic Peninsula: I–Sea ice, summer mixed layer, and irradiance. Deep-Sea Res. Part II Top. Stud. Oceanogr. **55**: 2068–2085. doi:10.1016/j.dsr2.2008.05.021

Wehrens, R., and J. Kruisselbrink. 2018. Flexible self-organizing maps in kohonen 3.0. J. Stat. Soft. **87**: 1–18. doi:10.18637/jss.v087.i07

## Acknowledgments

We thank all past and present Palmer LTER members for their dedication in the field and lab, and support crew for their assistance. This research was supported by NSF OPP Integrated Systems Science Program Award No. 1440435 to O.M.S. for the Palmer LTER, and NSF OPP Award Nos. 1043339 to N.C. and 1341479 to A.M for the DNA data set. J.S.B. was supported by NSF OPP Award Nos. 1846837 and 1821911, and a Simons Foundation Early Career Marine Microbial Investigator award.

## Conflict of Interest

None declared.

*Submitted 24 March 2020*
*Revised 23 November 2020*
*Accepted 05 January 2021*

*Associate editor: Heidi Sosik*